

Quantitative fluorescence spectroscopy in turbid media using fluorescence differential path length spectroscopy

Arjen Amelink
Bastiaan Kruijt
Dominic J. Robinson
Henricus J. C. M. Sterenberg

Erasmus Medical Centre Rotterdam
Department of Radiation Oncology
Center for Optical Diagnostics and Therapy
Rotterdam, The Netherlands 3000 CA

Abstract. We have developed a new technique, fluorescence differential path length spectroscopy (FDPS), that enables the quantitative investigation of fluorophores in turbid media. FDPS measurements are made with the same probe geometry as differential path length spectroscopy (DPS) measurements. Phantom measurements are performed for two fiber diameters (400 μm and 800 μm) and for a wide range of optical properties (μ'_s : 0 to 10 mm^{-1} ; μ_a : 0 to 2 mm^{-1}) to investigate the influence of the optical properties on the measured differential fluorescence signal. The differential fluorescence signal varies by a factor of 1.4 and 2.2 over the biologically relevant scattering range (0.5 to 5 mm^{-1}) for a given fluorophore concentration for 400 μm and 800 μm fibers, respectively. The differential fluorescence signal is attenuated due to absorption at the excitation wavelength following Lambert-Beer's law with a path length equal to the differential path length.

© 2008 Society of Photo-Optical Instrumentation Engineers. [DOI: 10.1117/1.2992132]

Keywords: fluorescence; optical properties; turbid media.

Paper 07468R received Nov. 19, 2007; revised manuscript received May 26, 2008; accepted for publication Jul. 15, 2008; published online Oct. 3, 2008.

1 Introduction

Noninvasive quantitative optical measurements of chromophore concentrations in tissue requires knowledge of the optical path length in the tissue. For most fiber-optic measurement geometries, the optical path length depends on the scattering coefficient μ_s and on the absorption coefficient μ_a . Since μ_s and μ_a both vary significantly in tissue, quantitative measurements prove to be difficult in tissue unless specific fiber-optic measurement geometries are chosen. For example, the optical pharmacokinetics spectroscopy (OPS) system developed by Mourant et al.¹ uses elastic scattering spectra of tissue to calculate the concentration of chromophores in tissue using a fiber-optic probe with a source–detector separation of 1.7 mm. The separation of 1.7 mm was chosen to minimize the dependence of the path length of the collected photons on scattering properties of tissue. For scattering parameters that are typical of tissue, the path length varies by less than 20% for a given background absorption. This method has been applied to the measurement of chemotherapy drug concentrations in tissue.² A drawback of this method is that the path length is sensitive to the (background) absorption coefficient of tissue. This means that the amount of measured absorption due to the target chromophore strongly depends on the local blood content and blood saturation. As a consequence, a measurement must be made prior to injection of the target chromophore, and only changes in concentration can be measured

assuming that the background absorption does not change in time. This makes OPS measurements difficult when a background reflectance spectrum cannot be acquired, and even more difficult to interpret when there are changes in the background absorption of tissue. Changes in background absorption can occur for a variety of reasons. Pressure between the measurement probe and the surface of the tissue can influence the blood content. Open surgical procedures can significantly influence both blood volume and saturation. Furthermore, changes in background absorption are a particular problem for *in vivo* photosensitizer concentration measurements during photodynamic therapy (PDT), when the background absorption can change dramatically due to changes in blood volume and saturation resulting from the therapy itself.³

Another technique that features a known path length is differential path length spectroscopy (DPS).^{4,5} The path length of photons contributing to the differential reflectance signal varies only slightly over a very broad range of both scattering and absorption coefficients. This facilitates quantitative concentration measurements even for strong variations in either absorption or scattering. However, chromophore concentrations calculated from elastic scattering measurements rely on (small) differences between large amounts of detected light with and without the chromophore present. Therefore, the combination of dynamic range and signal-to-noise of the elastic scattering measurement device becomes a limiting factor for accurate measurement of small concentrations of chromophores or measurements of chromophores with low absorption coefficients. This is particularly true for DPS, for

Address all correspondence to: A. Amelink, PhD, Center for Optical Diagnostics and Therapy, Department of Radiation Oncology, Erasmus MC, PO Box 2040, 3000 CA, Rotterdam, The Netherlands. Tel: +31 10 4632104; Fax: +31 10 4632141; E-mail: a.amelink@erasmusmc.nl

which the average path length of the measured photons is very small (approximately equal to the fiber diameter). In contrast, the dynamic range for fluorescence measurements is much larger than for scattering (absorption) measurements since the fluorescence is measured at a different wavelength than the excitation (scattered) light. For this reason, we have now developed a technique based on the principles of DPS (subtraction of the diffuse photons to obtain a well-defined measurement volume) but with the enhanced dynamic range of fluorescence measurements: fluorescence-DPS (FDPS).

Fluorescence emission from fluorophores is influenced by their environment. There exists a complex relationship between the concentration of a chromophore and its absorption cross section and fluorescence emission intensity. *In vivo* fluorescence (and to a lesser degree absorption) can be altered by many factors that include changes in quantum yield induced by changes in the microenvironment,⁶ photobleaching,⁷ biological compartmentalization, and alteration in binding and aggregation.^{8,9} In a turbid sample, the amount of fluorescence detected depends not only on the fluorophore concentration and quantum yield, but also on the scattering and absorption coefficients of the medium. Various algorithms and measurement geometries have been developed to correct for the influence of scattering and absorption on a measured fluorescence spectrum. Zhang et al.¹⁰ and Muller et al.¹¹ have used photon migration techniques to establish a very general algorithm that corrects for the influence of the optical properties on the measured fluorescence for any measurement geometry and for large variations in scattering and absorption. In this correction algorithm, the diffuse reflectance, measured in the same geometry as the fluorescence measurements, is used to correct for differences in tissue optical properties. Unfortunately, elaborate probe specific calibration procedures are required, and the correction algorithm is quite complex.

Several other authors have developed more simple correction algorithms based on specific probe geometries. Canpolat and Mourant¹² used various source-detector pairs to measure fluorescence and scattered excitation light for small source-detector separations. From Beer's law, they determined that their fluorescence-to-excitation reflectance ratio would be proportional to the product of fluorescence quantum yield, path length, and fluorophore absorption coefficient when the background absorption and scattering coefficients are the same at the excitation and emission wavelengths. Weersink et al.¹³ described a similar measurement technique, except that the fluorescence and reflected excitation light were measured at two different distances. Using a source-detector separation of 0.65 mm for fluorescence and 1.35 mm for reflectance measurements, they showed that it was possible to measure fluorophore concentrations to an accuracy of 15% over a wide range of optical properties using the fluorescence-to-reflectance ratio. In the measurement geometry of Pogue and Burke,¹⁴ fluorescence was excited and detected with a single small-diameter (100 μm) fiber, but the scattered excitation light was measured with an adjacent fiber. Measurements in phantoms showed that the fluorescence-to-reflectance ratio in this geometry varied by approximately 30% for a given fluorophore concentration over a broad range of optical properties. Diamond et al.¹⁵ also used a single small-diameter (200 μm) optical fiber to excite and detect the fluorescence and found that the uncorrected fluorescence signal was insen-

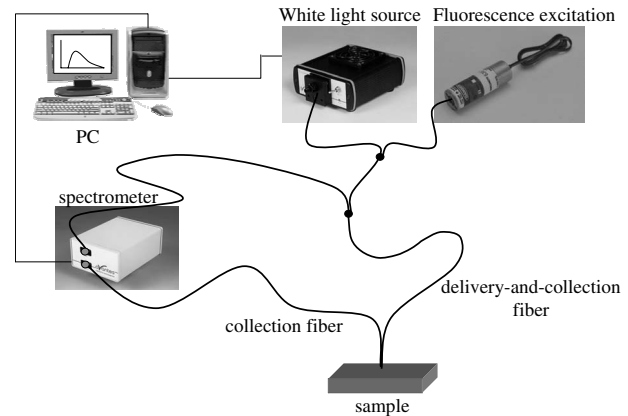


Fig. 1 Schematic diagram of the FDPS setup.

sitive to changes in the scattering coefficient and anisotropy as well as a limited range of absorption coefficients (up to 0.12 mm^{-1}) of the turbid samples, due to the small sampling volume of their technique. However, this single-fiber fluorescence method suffers from the same drawback as Mourant's reflectance method: the signal will be sensitive to larger changes in the (background) absorption coefficient of tissue. For wavelengths below 600 nm, the tissue absorption coefficient for most biological tissues is an order of magnitude larger than 0.12 mm^{-1} , mainly due to blood absorption.¹⁶ This limits the applicability of the present techniques to those chromophores that exhibit large absorption (and emission) bands in the red or near-infrared wavelength regions. Therefore, our objective here is to establish an algorithm that can be used to correct FDPS measurements for larger changes in the background absorption coefficient (as high as 2.0 mm^{-1}). Furthermore, we will show that FDPS measurements do not need to be corrected for changes in the reduced scattering coefficient in the range $0.5\text{--}5 \text{ mm}^{-1}$, which are values typically encountered in tissue.¹⁶⁻²⁰

2 Materials and Methods

2.1 Experimental Setup

The setup is an adapted version of a differential path length spectrometer and is shown schematically in Fig. 1. Light from a tungsten halogen lamp (Ocean Optics HL-2000) or a blue laser diode (Power Technology PPMT-LD1382, output 5 mW at 405 nm) is led through a 100- μm bifurcated optical fiber, which is at its distal end coupled to a 200- μm bifurcated optical fiber, which is at its distal end coupled to the 400- μm delivery-and-collection (dc) fiber. The distal end of the fiber probe is polished at an angle of 15 deg to minimize the collection of specularly reflected light at the probe-medium interface and contacts the sample under investigation. Reflected or fluorescent light collected by the dc fiber is coupled back into the 200- μm bifurcated fiber and coupled to the dc channel of a four-channel spectrometer (Ocean Optics MC-2000-4). Light reflected back from the sample into the other arm of the 400- μm bifurcated fiber-optic probe [the collection (c) fiber] is coupled into the c-channel of the four-channel spectrometer. The c-fiber and dc-fiber are touching to minimize the distance between them. Fluorescence and reflectance mea-

measurements were performed consecutively by switching on either the laser or the halogen lamp. An identical setup with twice as large fibers was connected to the third and fourth channels of the four-channel spectrometer. Measurements with the 400- μm FDPS probe and the 800- μm FDPS probe were performed consecutively. In the following, the difference of the dc- and c-fiber reflectance signals is called the *differential reflectance signal* \mathbf{DR} , where throughout this paper, a wavelength-dependent parameter will be presented in bold and parameters appearing in nonbold are implicitly assumed to be wavelength independent. Similarly, the difference in the fluorescence collected by the dc- and c-fibers is called the *differential fluorescence signal*, \mathbf{DF} .

2.2 Calibration

The total fluorescence intensity I_{sample}^F measured by the delivery-and-collection fiber in contact with a sample with the laser on can be written as:

$$I_{\text{sample}}^F = F_{\text{sample}}^{\text{dc}} \cdot T_{\text{dc}}, \quad (1)$$

where $F_{\text{sample}}^{\text{dc}}$ is the number of fluorescent photons collected by the dc-fiber and T_{dc} is the transmission function of the photons traveling from the tip of the delivery-and-collection fiber to the dc-spectrometer channel. Similarly, the total fluorescence intensity J_{sample}^F measured by the collection fiber is:

$$J_{\text{sample}}^F = F_{\text{sample}}^{\text{c}} \cdot T_{\text{c}}, \quad (2)$$

where $F_{\text{sample}}^{\text{c}}$ is the number of fluorescent photons collected by the c-fiber, and T_{c} is the transmission function of the photons traveling from the tip of the collection fiber to the c-spectrometer channel. The transmission functions T_{dc} and T_{c} are measured using a calibrated white light source (Ocean Optics HL-2000-CAL) for which the output of the lamp is known. For these measurements, the distal end of the probe, which was terminated with a SubMiniature version A (SMA) connector, was screwed in the SMA socket of the calibration lamp, and we measure $I_{\text{cal}} = L_{\text{cal}} \cdot T_{\text{dc}}$ and $J_{\text{cal}} = L_{\text{cal}} \cdot T_{\text{c}}$ where L_{cal} is the known output of the lamp.

Last, day-to-day variations in laser output from the distal end of the dc-fiber are measured by measuring the fluorescence intensity with the probe at a fixed distance from fluorescent spectralon (Labsphere USFS-200-010), which is a stable solid fluorescent standard. Alternatively, the output power of the laser can be directly measured by a power meter.

The differential fluorescence signal \mathbf{DF} is calculated by

$$\mathbf{DF} \equiv F_{\text{sample}}^{\text{dc}} - F_{\text{sample}}^{\text{c}} = L_{\text{cal}} \left(\frac{I_{\text{sample}}^F}{I_{\text{cal}}} - \frac{J_{\text{sample}}^F}{J_{\text{cal}}} \right). \quad (3)$$

The white light differential reflectance is measured as described previously^{4,5}:

$$\mathbf{DR} = c \left[\frac{(I - I_{\text{water}})}{(I_{\text{white}} - I_{\text{black}})} - \frac{J}{(J_{\text{white}} - J_{\text{black}})} \right], \quad (4)$$

where $(I - I_{\text{water}})$ represents the dc-fiber signal (I) corrected for internal reflections (I_{water}) using water in a dark reservoir. Fiber transmission characteristics and lamp spectra are accounted for by dividing the (corrected) I and J signals by

their reference reflections ($I_{\text{white}} - I_{\text{black}}$) and ($J_{\text{white}} - J_{\text{black}}$), and calibration constant c depends on the distance between the probe tips and the reference standards.

2.3 Phantoms

To characterize the differential fluorescence signal as a function of the optical properties, phantom measurements are performed. We have used liquid phantoms consisting of Intralipid 20% in different dilutions to vary the reduced scattering coefficient from 0 to 10 mm^{-1} at the excitation wavelength of 405 nm. To simulate the presence of an exogenous fluorophore, Sulforhodamine 101 was added to the phantoms in concentrations ranging from 0.2 μM to 20 μM . The fluorescence quantum yield of sulforhodamine dissolved in ethanol is 0.9.²¹ Last, background absorption at the excitation wavelength was varied from 0 to 2 mm^{-1} by addition of hemoglobin (Sigma-Aldrich, H2500) to the phantoms. Absorption at the sulforhodamine emission wavelengths ($\lambda > 550$ nm) is at least an order of magnitude smaller than at the excitation wavelength.

3 Results

3.1 Fluorophore Concentration Dependence

The differential fluorescence \mathbf{DF} consists of two components: Intralipid fluorescence and sulforhodamine fluorescence. Therefore, for all phantoms, the background fluorescence due to Intralipid was measured using phantoms with identical optical properties but without sulforhodamine and was, after normalization to the average differential fluorescence in the wavelength region $500 \text{ nm} < \lambda < 550 \text{ nm}$, subtracted from the \mathbf{DF} signal to obtain the sulforhodamine differential fluorescence.

Figure 2(a) shows \mathbf{DF} for a fixed reduced scattering coefficient of $\mu_s' = 1.5 \text{ mm}^{-1}$ at 405 nm and for different fluorophore concentrations c_F for the 400- μm FDPS system. Figure 2(b) shows \mathbf{DF} divided by fluorophore concentration c_F . The \mathbf{DF}/c_F ratios are constant both in size and in spectral shape, which implies that there is a linear relationship between the differential fluorescence and the fluorophore concentration. In the following, the area under the differential fluorescence curves in the wavelength region $550 \text{ nm} < \lambda < 700 \text{ nm}$, $\mathbf{DF} \equiv \int_{550}^{700} d\lambda \mathbf{DF}$, is analyzed as a function of the optical properties.

3.2 Measurement Reproducibility

We have tested the measurement reproducibility for phantoms with optical properties corresponding to the median of our measurement range ($\mu_s' = 1.5 \text{ mm}^{-1}$ and $\mu_a = 1.0 \text{ mm}^{-1}$). Three different sets of phantoms were made with the same optical properties, with and without sulforhodamine (i.e., $c_F = 0 \mu\text{M}$ and $c_F = 1 \mu\text{M}$). Furthermore, the effect of manual sample homogenization was investigated by measuring the phantoms after not shaking, gentle shaking, and vigorous shaking. The largest effects on the relative standard deviations of \mathbf{DF} and \mathbf{DR} were found to be due to the differences in shaking: $\Delta\mathbf{DF}/\mathbf{DF} \approx 7\%$ and $\Delta\mathbf{DR}/\mathbf{DR} \approx 2\%$ for the 400- μm FDPS system, and $\Delta\mathbf{DF}/\mathbf{DF} \approx 7\%$ and $\Delta\mathbf{DR}/\mathbf{DR} \approx 6\%$ for the 800- μm FDPS system. Here, the standard deviation in the differential reflectance ($\Delta\mathbf{DR}$) was calculated at

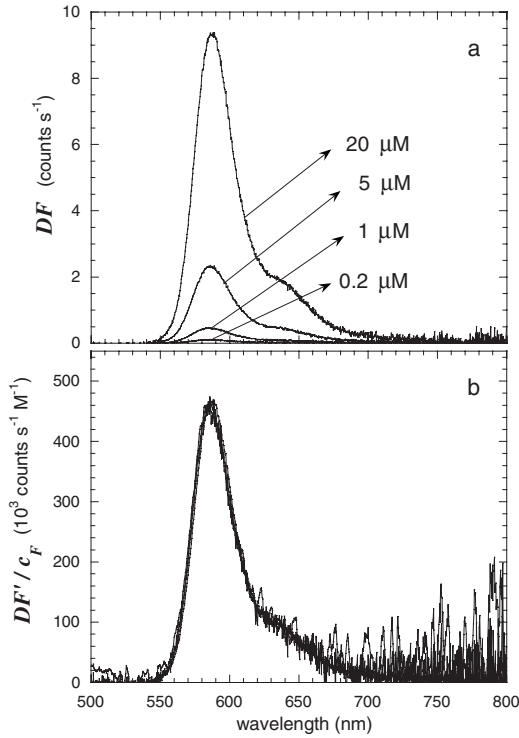


Fig. 2 (a) Measured differential fluorescence DF for different fluorophore concentrations c_F for a fixed scattering coefficient ($\mu'_s = 1.5 \text{ mm}^{-1}$), and (b) ratio of DF and c_F for the same measurements.

the excitation wavelength after normalization of the differential reflectance spectra DR in the wavelength region [460 to 500] nm, where hemoglobin absorption is very small compared to the absorption at the excitation wavelength of 405 nm. The relative standard deviation $\Delta DR/DR$ in the absence of hemoglobin, associated with homogenization (shaking) of the phantoms, was found to be 2% for both fiber diameters.

3.3 Scattering Dependence

Figure 3(a) shows DF for a fixed fluorophore concentration ($c_F = 1 \mu\text{M}$) for the 400- μm FDPS system, but now for different reduced scattering coefficients ($\mu'_s = 0.15, 0.30, 0.75, 1.5, 3.75,$ and 7.5 mm^{-1} at 405 nm). The error bars represent the 7% standard deviation corresponding to the measurement reproducibility. The differential fluorescence first decreases up to $\mu'_s = 1.5 \text{ mm}^{-1}$ and then increases with increasing scattering coefficient. In the range relevant for biological tissues ($0.5 \text{ mm}^{-1} < \mu'_s < 5 \text{ mm}^{-1}$),^{14–18} the maximum variation in differential fluorescence ($DF_{\text{max}}/DF_{\text{min}}$) equals a factor of 1.4. Figure 3(b) shows the same data for the 800- μm FDPS system, which shows a similar pattern, but the increase in differential fluorescence already starts at $\mu'_s = 0.75 \text{ mm}^{-1}$. In this case, the maximum variation in differential fluorescence ($DF_{\text{max}}/DF_{\text{min}}$) equals a factor of 2.2 in the range relevant for biological tissues.

3.4 Background Absorption Dependence

Figure 4(a) shows DF for a fixed fluorophore concentration ($c_F = 1 \mu\text{M}$) and a fixed scattering coefficient (μ'_s

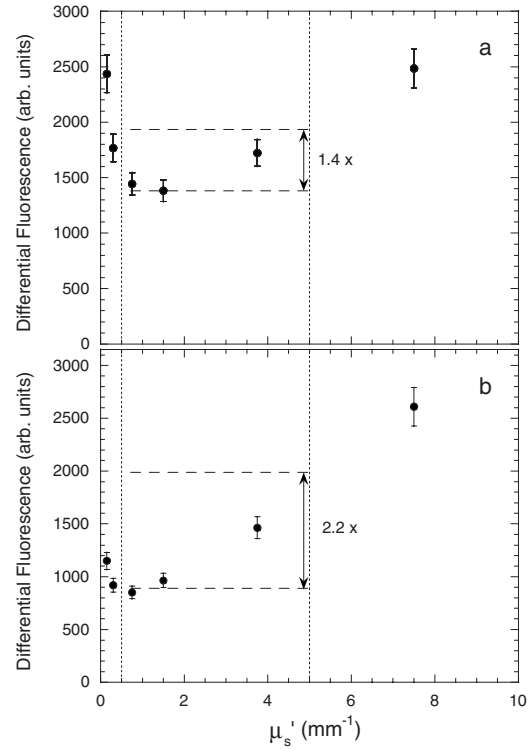


Fig. 3 Measured differential fluorescence DF as a function of reduced scattering coefficient for a fixed fluorophore concentration ($c_F = 1 \mu\text{M}$), (a) for the 400- μm FDPS probe, and (b) for the 800- μm FDPS probe.

$= 0.75 \text{ mm}^{-1}$ at 405 nm) for the 400- μm FDPS system as a function of the background absorption coefficient at the excitation wavelength. The error bars represent the 7% standard deviation corresponding to the measurement reproducibility. The differential fluorescence decreases strongly with increasing background absorption. Therefore, it is necessary to correct the measured differential fluorescence for these high background absorptions. Previously, we have shown that the white light differential reflectance is attenuated due to absorption following Beer's law according to Eq. (5).^{4,5}

$$DR(\mu_a) = DR(0) \exp(-\tau_{dps} \mu_a), \quad (5)$$

where τ_{dps} is the differential path length. Since the differential fluorescence is measured with exactly the same fiber-optic geometry, we will assume that the differential fluorescence is attenuated according to Eq. (6):

$$DF(\mu_{a,x}) = DF(0) \exp(-\tau_{dps} \mu_{a,x}). \quad (6)$$

Combining Eqs. (5) and (6), we can write,

$$DF(0) = DF(\mu_{a,x}) \frac{DR_x(0)}{DR_x(\mu_{a,x})}, \quad (7)$$

where $DR_x(\mu_{a,x})$ and $DR_x(0)$ are the differential reflectance signals at the excitation wavelength measured with and without background absorber present, respectively. The ratio of $DR_x(0)$ and $DR_x(\mu_{a,x})$ was calculated after normalization of the differential reflectance spectra DR for the different concentrations of hemoglobin in the wavelength region

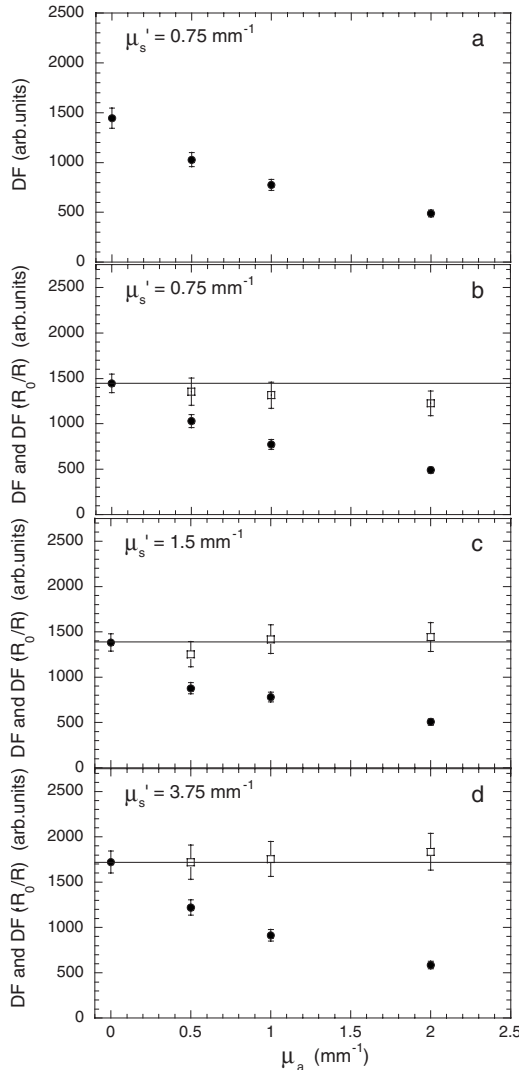


Fig. 4 (a) Measured differential fluorescence DF as a function of absorption coefficient for a fixed fluorophore concentration ($c_F = 1 \mu\text{M}$) and a fixed reduced scattering coefficient ($\mu_s' = 0.75 \text{ mm}^{-1}$) for the 400- μm FDPS probe. (b) The same, including the corrections calculated according to Eq. (7) (open squares). (c) The same for $\mu_s' = 1.5 \text{ mm}^{-1}$, and (d) the same for $\mu_s' = 3.75 \text{ mm}^{-1}$.

[460 to 500] nm, where hemoglobin absorption is very small compared to the absorption at the excitation wavelength of 405 nm. The open squares in Fig. 4(b) represent the calculations of $DF(0)$ according to Eq. (7). The error bars on the open squares represent the standard deviations corresponding to the measurement uncertainties associated with DF , $DR_x(0)$, and $DR_x(\mu_{a,x})$, i.e., $\Delta DF(0)/DF(0) = \Delta DF(\mu_{a,x})/DF(\mu_{a,x}) + \Delta DR_x(0)/DR_x(0) + \Delta DR_x(\mu_{a,x})/DR_x(\mu_{a,x}) = 7\% + 2\% + 2\% = 11\%$. Good agreement between calculation and measurement is observed, except for the highest absorption coefficient, where a small deviation is observed. Figures 4(c) and 4(d) show similar plots for the $\mu_s' = 1.5 \text{ mm}^{-1}$ and $\mu_s' = 3.75 \text{ mm}^{-1}$ at 405-nm cases, respectively, for the 400- μm FDPS system. Last, Figs. 5(a)–5(c) show similar plots for the $\mu_s' = 0.75 \text{ mm}^{-1}$, $\mu_s' = 1.5 \text{ mm}^{-1}$, and $\mu_s' = 3.75 \text{ mm}^{-1}$ at 405-nm cases, respec-

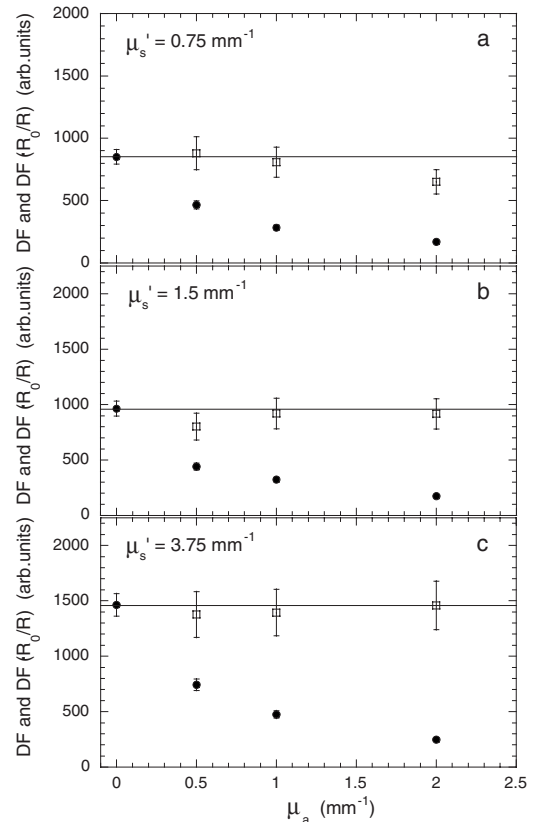


Fig. 5 Measured differential fluorescence DF (solid circles) as a function of absorption coefficient for a fixed fluorophore concentration ($c_F = 1 \mu\text{M}$) and the corrections calculated according to Eq. (7) (open squares) for the 800- μm FDPS probe, for (a) $\mu_s' = 0.75 \text{ mm}^{-1}$, (b) $\mu_s' = 1.5 \text{ mm}^{-1}$, and (c) $\mu_s' = 3.75 \text{ mm}^{-1}$.

tively, for the 800- μm FDPS system. In this case, the error bars on the open squares are slightly larger (15%) due to the larger measurement uncertainty associated with $DR_x(\mu_{a,x})$.

4 Discussion and Conclusion

We have adapted our DPS technique to include fluorescence measurements (FDPS) to enable quantitative fluorescence spectroscopy in turbid media. We showed that the differential fluorescence signal increases linearly with fluorophore concentration for a fixed scattering and background absorption coefficient (Fig. 2). This facilitates a straightforward interpretation of the fluorescence signals for this range of fluorophore concentrations. We found deviations from linearity for fluorophore concentrations above 50 μM (data not shown). All our subsequent measurements were performed for a concentration of 1 μM , which is well below this value.

We investigated the scattering dependence of the differential fluorescence signal. We found that the differential fluorescence signal decreases up to a reduced scattering coefficient of 1.5 mm^{-1} in case of 400- μm fibers and then increases with increasing scattering coefficient [Fig. 3(a)]. Most likely, this is due to a combined effect of two counteractive mechanisms:

- The volume over which the DF (and DR) is collected is proportional to the differential path length, which decreases

strongly with increasing scattering for very low reduced scattering coefficients and becomes roughly constant in the biologically relevant range.^{4,5}

- The fluence rate in the **DF** (and **DR**) collection volume increases with increasing scattering coefficient due to increased backscattering of the excitation light.

These two effects result in an initial decrease followed by a subsequent steady increase in the differential fluorescence signal. Since the collection volume (or differential path length) for 800- μm fibers becomes constant for lower scattering coefficients compared to 400- μm fibers,⁵ the increase in differential fluorescence already starts at a reduced scattering coefficient of 0.75 mm^{-1} for the 800- μm fibers [Fig. 3(b)].

In the scattering range relevant for biological tissues, the maximum variation in differential fluorescence ($DF_{\text{max}}/DF_{\text{min}}$) equals a factor of 1.4 for the 400- μm FDPS system and a factor of 2.2 for the 800- μm FDPS system. Note that these factors represent the maximum variation over an order of magnitude change in scattering. For any specific target tissue, the scattering coefficient at the excitation wavelength will vary much less than an order of magnitude; a very conservative estimate would be a twofold variation at the most.¹⁶ Even variations in scattering as large as a factor of 2 result in a maximum variation in differential fluorescence of only a factor of 1.16 for the 400- μm FDPS system and a factor of 1.35 for the 800- μm FDPS system. This implies that FDPS measurements performed on specific target organs can be well compared to each other without correcting for scattering differences, while a more careful interpretation is necessary when FDPS measurements on different organs (with very different scattering coefficients) are to be compared.

The fluence rate in the **DF** collection volume will be attenuated due to absorption according to Beer's law similar to the differential reflectance **DR**, since they are measured in the same geometry. This can be used to account for the effects of absorption on **DF** through Eq. (7), which employs the ratio of differential reflectance signals measured with and without absorber present [$DR_x(\mu_{a,x})$ and $DR_x(0)$, respectively]. Figures 4 and 5 show that this correction works very well, apart from the combination of very low scattering and very high absorption, where a small deviation can be observed. A possible explanation for this deviation may be that our model does not account for absorption at the emission wavelengths. The largest effect of absorption at the emission wavelengths will be found for the highest concentration of hemoglobin, i.e., for the highest absorption coefficient at the excitation wavelength, combined with the longest differential path length τ_{dps} , i.e., the lowest scattering coefficient.⁵

In this phantom study, we could measure both $DR_x(\mu_{a,x})$ and $DR_x(0)$ directly, while in tissue, only $DR_x(\mu_{a,x})$ can be measured. Importantly, in that case, $DR_x(0)$ can still be extracted from the measured wavelength dependence of the differential reflectance **DR** by fitting the complete DPS spectrum to our previously developed model²²⁻²⁵ and subsequently calculating what the differential reflectance at the excitation wavelength should be in the absence of blood, as discussed in the following. Our general model [Eq. (5)] can, in case of tissue measurements, be written as²²⁻²⁵

$$DR(\mu_a) = \left[a_1 \left(\frac{\lambda}{\lambda_0} \right)^{a_2} + a_3 \left(\frac{\lambda}{\lambda_0} \right)^{-4} \right] \cdot \exp(-\tau_{\text{dps}} \mu_a^{\text{total}}). \quad (8)$$

The scattering function of tissue (in square brackets) is modeled by a combination of Mie scattering and Rayleigh scattering, given by power law functions with amplitudes a_1 and a_3 and wavelength dependencies $(\lambda/\lambda_0)^{a_2}$ and $(\lambda/\lambda_0)^{-4}$, respectively. Here, λ_0 is a normalization wavelength, which we usually set to 800 nm. The absorption coefficient μ_a^{total} is the sum of the absorption coefficients of all the chromophores present in the interrogation volume, which in the visible wavelength region is typically only blood:

$$\mu_a^{\text{total}} = a_4 \cdot [a_5 \cdot \mu_a^{\text{HbO}_2} + (1 - a_5) \cdot \mu_a^{\text{Hb}}] \cdot \left(\frac{1 - \exp\{-a_6 \cdot [a_5 \cdot \mu_a^{\text{HbO}_2} + (1 - a_5) \cdot \mu_a^{\text{Hb}}]\}}{a_6 \cdot [a_5 \cdot \mu_a^{\text{HbO}_2} + (1 - a_5) \cdot \mu_a^{\text{Hb}}]} \right). \quad (9)$$

Parameter a_4 is the blood volume fraction, a_5 is the blood oxygenation, and a_6 is the average vessel diameter. Input spectrum $\mu_a^{\text{HbO}_2}$ is the absorption coefficient of fully oxygenated whole blood, and μ_a^{Hb} is the absorption coefficient of fully deoxygenated whole blood. When the measured DPS spectrum is fitted to the model [Eqs. (8) and (9)] using least-squares minimization, we obtain best estimates for the fit parameters $a_1 - a_6$. Using the best estimates of the scattering parameters $a_1 - a_3$, $DR_x(0)$ can be calculated by

$$DR_x(0) = a_1 \left(\frac{\lambda_x}{\lambda_0} \right)^{a_2} + a_3 \left(\frac{\lambda_x}{\lambda_0} \right)^{-4}. \quad (10)$$

Thus, although our correction algorithm [Eq. (7)] utilizes only the differential reflectance at the excitation wavelength, measurement of the complete differential reflectance spectrum is required to estimate $DR_x(0)$ accurately. Furthermore, it follows from this analysis that our correction algorithm can in principle correct for background absorption at any excitation wavelength, provided that the absorption coefficients of all the absorbing molecules are known such that $DR_x(0)$ can be estimated accurately using the previously described fitting routine.

In this phantom study, a single exogenous fluorophore was used to study the influence of the optical properties on the FDPS signal. However, our technique can be applied to any number of endogenous as well as exogenous fluorophores. Of particular interest could be the study of native tissue fluorescence of neoplastic epithelial tissues using FDPS, where the small sampling depth of FDPS allows sensitive measurements of potential changes in the concentration of epithelial fluorophores involved in the cellular metabolism such as NADH.

The presence of background absorption is an important parameter to consider both in quantitative fluorescence and in elastic scattering spectroscopic measurements. Even when the path length of measured photons varies little with scattering coefficient, the path length will still depend on the absorption coefficient. In the measurement geometry of Canpolat and Mourant¹² and Diamond et al.¹⁵ (fluorescence) or Mourant et al.¹ (absorption), the background absorption dependence of

the signals reduces the validity range of their approach to only small variations in the background absorption coefficient, and generally to the red and near-infrared wavelength regions. For quantitative fluorescence measurements with excitation in the blue or green wavelength regions, a measurement technique is needed that does not depend so heavily on background absorption, since the absorption coefficient of tissue in these wavelength regions is much higher and may vary significantly within the target tissue. Therefore, the advantage of FDPS over other quantitative fluorescence measurements is its capability to deal with large variations in background absorption using a simple correction algorithm. This makes FDPS especially valuable for *in vivo* photosensitizer fluorescence spectroscopy during PDT, when the background absorption at these wavelengths can change dramatically. Note that the scattering coefficient is not expected to vary by more than a factor of 2 during PDT^{3,26} and will therefore have a small influence on the FDPS signal.

Another advantage of FDPS is that the collection volume can be adjusted to match the relevant dimensions of the application. For absolute fluorescence measurements of photosensitizers or chemotherapy drugs that preferentially localize at specific depths in the tissue, it is essential to selectively interrogate the relevant tissue volume and to avoid averaging drug concentrations over larger/smaller volumes by probing too deep/shallow in the tissue. With FDPS, this can be achieved by choosing the appropriate fiber diameter since the collection volume is proportional to the fiber diameter.⁵

Another potential advantage of FDPS is that no matter which fiber diameter is used, the measurement volume is always relatively small. Hence, multiple FDPS measurements can be used to obtain information about the often heterogeneous distribution of fluorophores in larger tissue volumes.²⁷ Last, FDPS is of particular interest for monitoring PDT since a DPS measurement, apart from correcting the differential fluorescence for background absorption changes, also gives information about other important PDT parameters such as the local oxygen saturation, blood volume, and changes in scattering. The most appropriate applications of FDPS are likely to be associated with superficial (or intraluminal) PDT.²⁶ Here, combinations of fiber diameters can also serve to interrogate and compare different tissue volumes. Therefore, we believe that combining the FDPS and DPS measurements during PDT will give valuable information regarding the PDT process.

Acknowledgments

This research is supported by the Dutch Technology Foundation STW, applied science division of NWO and the Technology Program of the Ministry of Economic Affairs, and by the NIH, Grant No. NIH/NCI U54 CA104677.

References

1. J. R. Mourant, I. J. Bigio, D. A. Jack, T. M. Johnson, and H. D. Miller, "Measuring absorption coefficients in small volumes of highly scattering media: source-detector separations for which path lengths do not depend on scattering properties," *Appl. Opt.* **36**, 5655–5661 (1997).
2. J. R. Mourant, T. M. Johnson, G. Los, and I. J. Bigio, "Noninvasive measurement of chemotherapy drug concentrations in tissue: preliminary demonstrations of *in vivo* measurement," *Phys. Med. Biol.* **44**, 1397–1417 (1999).

3. A. Amelink, A. van der Ploeg-van den Heuvel, W. J. de Wolf, D. J. Robinson, and H. J. C. M. Sterenberg, "Monitoring PDT by means of superficial reflectance spectroscopy," *J. Photochem. Photobiol., B* **79**, 243–251 (2005).
4. A. Amelink and H. J. C. M. Sterenberg, "Measurement of the local optical properties of turbid media using differential path length spectroscopy," *Appl. Opt.* **43**, 3048–3054 (2004).
5. O. P. Kaspers, H. J. C. M. Sterenberg, and A. Amelink, "Controlling the optical path length in turbid media using differential path length spectroscopy: fiber diameter dependence," *Appl. Opt.* **47**, 365–371 (2008).
6. B. C. Wilson, M. S. Patterson, and L. Lilge, "Implicit and explicit dosimetry in photodynamic therapy: a new paradigm," *Lasers Med. Sci.* **12**, 182–199 (1997).
7. D. J. Robinson, H. S. de Bruijn, N. van der Veen, M. R. Stringer, S. B. Brown, and W. M. Star, "Fluorescence photobleaching of ALA-induced protoporphyrin IX during photodynamic therapy of normal hairless mouse skin: the effect of light dose and irradiance and the resulting biological effect," *Photochem. Photobiol.* **67**, 140–149 (1998).
8. K. Woodburn, C. K. Chang, S. Lee, B. Henderson, and D. Kessel, "Biodistribution and PDT efficacy of a ketochlorin photosensitizer as a function of the delivery vehicle," *Photochem. Photobiol.* **60**, 154–159 (1994).
9. B. Aveline, T. Hasan, and R. W. Redmond, "Photophysical and photosensitizing properties of benzoporphyrin derivative monoacid ring A (BPD-MA)," *Photochem. Photobiol.* **59**, 328–335 (1994).
10. Q. Zhang, M. G. Muller, J. Wu, and M. S. Feld, "Turbidity-free fluorescence spectroscopy of biological tissue," *Opt. Lett.* **25**, 1451–1453 (2000).
11. M. G. Muller, I. Georgakoudi, Q. Zhang, J. Wu, and M. S. Feld, "Intrinsic fluorescence spectroscopy in turbid media: disentangling effects of scattering and absorption," *Appl. Opt.* **40**, 4633–4646 (2001).
12. M. Canpolat and J. R. Mourant, "Monitoring photosensitizer concentration by use of a fiber-optic probe with a small source-detector separation," *Appl. Opt.* **39**, 6508–6514 (2000).
13. R. Weersink, M. S. Patterson, K. Diamond, S. Silver, and N. Padgett, "Noninvasive measurement of fluorophore concentration in turbid media with a simple fluorescence/reflectance ratio technique," *Appl. Opt.* **40**, 6389–6395 (2001).
14. B. W. Pogue and G. Burke, "Fiber-optic bundle design for quantitative fluorescence measurement from tissue," *Appl. Opt.* **37**, 7429–7436 (1998).
15. K. R. Diamond, M. S. Patterson, and T. J. Farrell, "Quantification of fluorophore concentration in tissue-simulating media by fluorescence measurements with a single optical fiber," *Appl. Opt.* **42**, 2436–2442 (2003).
16. A. J. Welch and M. J. C. van Gemert, Eds., *Optical-Thermal Response of Laser Irradiated Tissue*, pp. 280–300 (Plenum, New York, 1995).
17. R. M. P. Doornbos, R. Lang, M. C. Aalders, F. W. Cross, and H. J. C. M. Sterenberg, "The determination of *in vivo* human tissue optical properties and absolute chromophore concentrations using spatially resolved steady-state diffuse reflectance spectroscopy," *Phys. Med. Biol.* **44**, 967–981 (1999).
18. N. Ghosh, S. K. Mohanty, S. K. Majumder, and P. K. Gupta, "Measurement of optical transport properties of normal and malignant human breast tissue," *Appl. Opt.* **40**, 176–184 (2001).
19. J. B. Fishkin, O. Coquoz, E. R. Anderson, M. Brenner, and B. J. Tromberg, "Frequency-domain photon migration measurements of normal and malignant tissue optical properties in a human subject," *Appl. Opt.* **36**, 10–20 (1997).
20. J. Qu, C. MacAulay, S. Lam, and B. Palcic, "Optical properties of normal and carcinomatous bronchial tissue," *Appl. Opt.* **33**, 7397–7405 (1994).
21. R. R. Birge, "Kodak laser dyes," Kodak publication JJ-169, Eastman Kodak Company, Rochester, NY (1987).
22. A. Amelink, M. P. L. Bard, J. A. Burgers, and H. J. C. M. Sterenberg, "*In vivo* measurement of the local optical properties of tissue using differential path length spectroscopy," *Opt. Lett.* **29**, 1087–1089 (2004).
23. M. P. L. Bard, A. Amelink, V. Noordhoek Hegt, W. J. Graveland, H. J. C. M. Sterenberg, H. C. Hoogsteden, and J. G. J. V. Aerts, "Measurement of hypoxia-related parameters in bronchial mucosa by use

- of optical spectroscopy," *Am. J. Respir. Crit. Care Med.* **171**, 1178–1184 (2005).
24. R. L. P. van Veen, A. Amelink, M. Menke-Pluymers, C. van der Pol, and H. J. C. M. Sterenberg, "Optical biopsy of breast tissue using differential path length spectroscopy," *Phys. Med. Biol.* **50**, 2573–2581 (2005).
 25. A. Amelink, O. P. Kaspers, H. J. C. M. Sterenberg, J. E. van der Wal, J. L. Roodenburg, and M. J. H. Witjes, "Non-invasive measurement of the morphology and physiology of oral mucosa by use of optical spectroscopy," *Oral Oncol.* **44**, 65–71 (2008).
 26. B. Kruijt, H. S. de Bruijn, A. van der Ploeg-van den Heuvel, R. W. F. de Bruin, H. J. C. M. Sterenberg, A. Amelink, and D. J. Robinson, "Monitoring ALA-induced PpIX-photodynamic therapy in the rat esophagus using fluorescence and reflectance spectroscopy," *Photochem. Photobiol.* (in press 2008).
 27. S. Mitra, E. Maugain, L. Bolotine, F. Guillemin, and T. H. Foster, "Temporally and spatially heterogeneous distribution of mTHPC in a murine tumor observed by two-color confocal fluorescence imaging and spectroscopy in a whole-mount model," *Photochem. Photobiol.* **81**, 1123–1130 (2005).